Wavelength-dependent collective effects in the multiphoton ionization of atomic deuterium

B. J. Shortt,[1,*] P. J. M. van der Burgt,[1] F. Giammanco,[2] J. A. Slevin,[1] and W. Lanigan[1]
[1]*Department of Experimental Physics, National University of Ireland, Maynooth, County Kildare, Ireland*
[2]*Instituto Nazionale di Fisica della Materia e Dipartimento di Fisica, Università di Pisa, 56126 Pisa, Italy*
(Received 5 March 2002; published 16 October 2002)

This paper presents the results of an experimental investigation into collective effects in the transient plasma formed by multiphoton ionization of atomic deuterium with a pulsed laser. The laser wavelength is varied in a narrow range around 243 nm, so that the photoionization is resonant with the metastable $2S_{1/2}$ state. The ion yield, the ion time-of-flight spectra, and the yield of Lyman-α photons have been measured as a function of laser intensity (from 1 to 340 MW/cm^2) and laser detuning around the $1S_{1/2}$-$2S_{1/2}$ two-photon resonance. During and shortly after the laser pulse, collective effects resulting from the mutual interaction of the photoelectrons and the ions affect the spatial and temporal distribution of the ions. Because of the near-degeneracy of the $2S_{1/2}$, $2P_{1/2}$, and $2P_{3/2}$ states, the resonant multiphoton ionization is affected by the Stark mixing of these states in the collective field. As a result, the time-dependent yields of ions and of Lyman-α photons are modulated by the interplay of the multiphoton ionization of the atoms and the collective effects in the plasma. From the measurements it is deduced that collective effects are important above a critical charge density of 3×10^8 ions/cm^3. An asymmetry is observed in the line profile of the total ion yield as a function of laser detuning. This asymmetry is interpreted to be due to the effect of the collective field upon the intermediate resonant $2S_{1/2}$ state of the photoionization process.

DOI: 10.1103/PhysRevE.66.046411 PACS number(s): 52.50.Jm, 32.80.Rm, 32.80.Wr

I. INTRODUCTION

In ionization experiments the production of a large number of electron-ion pairs in a small interaction volume can lead to high charge densities. Due to the different mobilities of the electrons and ions, large electric fields can be generated. These fields result in collective or space-charge effects that affect both the actual atomic process (production phase) and the recorded experimental results (collection phase). Reviews of the topic are provided by Giammanco and Spinelli [1] and by Ammosov [2]. The study of collective effects is a worthwhile task from two perspectives. First, it is important for experimenters to be able to verify that they are working in a regime where their results are not affected by collective interactions. Second, collective effects provide a rich mixture of phenomena from different fundamental disciplines such as atomic and plasma physics, and are worth studying in their own right. Collective effects have been observed in multiphoton ionization (MPI) of deuterium [3] and sodium [4–6], and in MPI and above-threshold ionization (ATI) of xenon [7–13]. Other areas where collective effects can be relevant are electron impact ionization of atoms [14–16], the nonlinear surface photoeffect [17], Coulomb expansion of molecules and clusters [18], higher-order harmonic generation [19], laser ablation [20], annealing, surface sputtering, and gas discharges [21,22]. Theoretical models for collective interactions have been developed by Giammanco and co-workers [19,23,24] and by Ammosov and co-workers [2,25]. A recent discussion of fundamental aspects and applications of low-temperature plasmas is given by Hippler *et al.* [26].

In the present experiment we study transient plasmas formed by multiphoton ionization of deuterium atoms. Deuterium presents an ideal situation for the study of collective effects. Deuterium is almost the lightest atom in the Periodic Table, so deuterium ions are very susceptible to the collective electric field in the transient plasma. The multiphoton ionization is resonant with the $2S_{1/2}$ metastable state of deuterium, so that the collective field Stark mixes the $2S_{1/2}$ state with the $2P_{1/2}$ and $2P_{3/2}$ states, thereby affecting the multiphoton ionization process. As a result two interactions are relevant to the time evolution of the plasma: (1) the collective interaction between the photoelectrons and the ions, and (2) the coupling between the multiphoton ionization process and the collective electric field in the plasma.

Contrary to these interactions, collisions of electrons and ions with neutral atoms (either in the ground state or in a metastable excited state) are not relevant. In our experiment the density n of neutral atoms is 10^{12} cm^{-3}, and for electrons with kinetic energies of a few eV colliding with ground state atoms the collision cross section σ is less than about 10^{-14} cm^2, so that the mean free path $\lambda=(n\sigma)^{-1}$ is larger than 1 m. For electrons colliding with excited neutral atoms the cross section can be as large as 10^{-13} cm^2 [27], but the excited state density is much lower than the density of ground state atoms.

The collective interactions in the MPI transient plasma have significant effects on the observed ion signals. In the initial part of the laser pulse the electron and ion clouds overlap. Due to the different mobilities of the electrons and the ions, the electron cloud expands very rapidly, thus inducing a fast growth of the collective field. (In our experiment the velocity of a photoelectron of 1.7 eV is 7.7×10^5 m/s as compared with 1.6×10^3 m/s for a deuterium ion at room temperature.) Immediately after the start of the laser pulse, the photoelectrons start to leave the volume occupied by the

*Present address: Atomic and Molecular Collisions Team, MS 121-104, Jet Propulsion Laboratory, 4800 Oak Grove Drive, Pasadena, CA 91109-8099.

ions, resulting in a non-neutral plasma. The ion mutual repulsion causes Coulomb expansion of the ion cloud. This has two effects on the observed ion signal. First, many ions may be lost due to the spatial dimensions of the ion cloud exceeding those of the entrance aperture of the ion detection system. This leads to anomalous saturation [3–6], at much lower laser intensities than expected on the basis of independent particle behavior. Second, during the expansion of the ion cloud some of the ions are pushed towards the ion detector and some are pushed away. This causes the ion time-of-flight profile to expand in time, and the initial ions to arrive at the ion detector at earlier times [3,4,13]. Both effects strongly depend on the total charge density produced in the focal volume of the laser and therefore on the laser intensity.

The ion signals are not solely determined by the Coulomb expansion of the ion cloud. Both the collective interaction between the photoelectrons and the ions and the coupling between the multiphoton ionization process and the collective field affect the density and spatial distribution of the ions in the initial stages of the plasma evolution and thereby affect the observed signals.

Even at low charge densities, in the absence of electron trapping, the electrons play an important role in the transient plasma. During and shortly after the laser pulse, the coupling between the electrons and the ions results in the oscillation of the width of the electron cloud around the ion cloud. Because the ion expansion is very slow, the frequency of oscillation is directly related to the electron plasma frequency [4,23]. In numerical simulations of MPI transient plasmas of deuterium [3], oscillatory structures have been observed in the Lyman-α photons emitted due to quenching of the $2S_{1/2}$ state in the collective field during and shortly after the laser pulse. These oscillations are directly related to the oscillations of the electron cloud in the transient plasma. At higher charge densities, the collective field may become so strong that many of the photoelectrons may become trapped [4].

During the laser pulse the coupling between the multiphoton ionization process and the collective electric field is relevant. In the experiments on atomic deuterium reported in this paper and also by Bowe *et al.* [3] the photoionization process is resonant with the $2S_{1/2}$ metastable state of deuterium. Bowe *et al.* [3] performed measurements of the Lyman-α photons emitted when the $2S_{1/2}$ state was quenched in the collective field of the transient plasma. In their measurements they observed a strong Lyman-α signal during the laser pulse before the extraction field was switched on. These measurements demonstrated the existence of collective fields of several hundred V/cm and provided direct evidence for the effect of the collective field on the multiphoton ionization of the atoms.

This paper presents the results of a study of the *wavelength dependence* of the collective effects in the transient plasma formed by multiphoton ionization of atomic deuterium. Whereas Bowe *et al.* [3] performed measurements exclusively on resonance, we are presenting measurements of the ion time-of-flight profiles, total ion yields, and Lyman-α photon yields as a function of laser detuning around the $1S_{1/2}$-$2S_{1/2}$ two-photon resonance. The purpose of these measurements is to specifically investigate the coupling between the multiphoton ionization of the atoms and the collective effects in the plasma, caused by the Stark mixing of the $2S_{1/2}$, $2P_{1/2}$, and $2P_{3/2}$ states in the collective field. In Sec. II of this paper we describe the experimental techniques used; in Sec. III we give a systematic presentation of the results, and in Sec. IV an interpretation and a discussion of the experimental results are given. A summary and conclusions are presented in Sec. V.

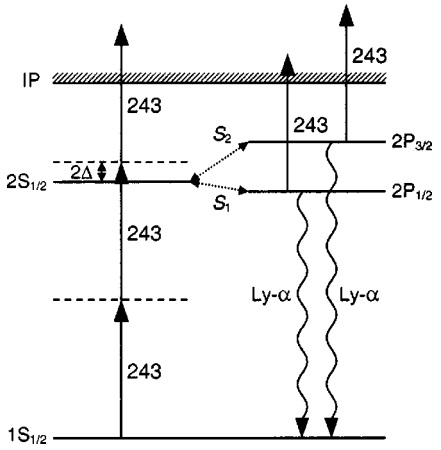

FIG. 1. Schematic energy level diagram of a deuterium atom in a laser field with a wavelength of 243 nm. S_1 and S_2 indicate the Stark couplings due to the total electric field in the interaction region, which is the sum of the ion extraction field and the collective field of the laser-produced plasma.

II. EXPERIMENT

A detailed description and diagram of the experimental setup can be found in [3]. The pulsed laser beam is produced by an excimer-dye laser system and has a wavelength of 243 nm. This beam is focussed into a vacuum chamber where it is crossed at 90° with an atomic deuterium beam, at a target density of approximately 10^{12} atoms/cm^3, produced by a radio frequency driven plasma discharge tube. The tube is fed with molecular deuterium through a palladium finger.

The products of the interaction are detected for each laser pulse. Ions are collected by an extraction field, which can be turned on before the laser pulse (advanced field) or immediately after the laser pulse (delayed field). The ions are guided by a series of focusing, drift, and deflecting electrodes to a pair of stacked microchannel plates. The Lyman-α photons are collimated by a magnesium fluoride lens and pass through an interference filter with peak transmission at the Lyman-α line to prevent scattered 243 nm photons from entering the detector. The Lyman-α photons are detected by a twin microchannel plate assembly similar to that used for the ion detection. The detectors are housed inside a vacuum chamber, which is pumped by a turbo/rotary pump combination to a base pressure of about 10^{-6} mbar (with the deuterium beam on).

An energy level diagram depicting the photoionization of atomic deuterium is shown in Fig. 1. In the experiment the laser wavelength is tuned to 243 nm so that the photoionization is resonant with the $2S_{1/2}$ state. Absorption of two laser

photons at 243 nm excites the atom to the metastable $2S_{1/2}$ state, from where the atom can either absorb a third photon to become ionized, or decay to the $1S_{1/2}$ ground state via the spontaneous emission of a Lyman-α photon at 121.6 nm. A channel for relaxation of the excited state via spontaneous emission is opened when the $2S_{1/2}$ state is Stark mixed with the close-lying $2P_{1/2}$ and $2P_{3/2}$ levels by an electric field in the interaction region. A photon signal observed in the case of a delayed ion extraction field is unambiguously attributable to the collective field in the transient plasma.

The data acquisition allows simultaneous real-time capture of both ion and photon signals and the laser energy on a shot-to-shot basis. The master signal for the timing of the experiment is provided by a trigger pulse generated by the dye laser control electronics approximately 600 ns before the excimer fires. This pulse is used for arming the acquisition electronics and pulsing the extraction field relative to the laser pulse. The jitter between the trigger pulse and the actual firing of the excimer is of the order of 5 ns. During all measurements the laser was operated at a low repetition rate (typically 1–5 Hz) in order to keep this jitter to a minimum and to ensure good intensity stability. The ion and photon signals are recorded by a two-channel digital oscilloscope, and the laser energy is recorded by a calibrated photodiode and/or by an energy meter. All three of these devices are interfaced to two data acquisition computers.

Two different measurement techniques have been employed to record the data. The first technique involved scanning the wavelength of the laser across the $1S_{1/2}$-$2S_{1/2}$ resonance and recording the ion and photon temporal signals as a function of the wavelength. The second technique involved setting the laser to a fixed wavelength in the vicinity of the $1S_{1/2}$-$2S_{1/2}$ resonance and recording the ion and photon temporal signals as a function of laser intensity.

Wavelength scans were performed covering a wavelength range from 243.00 nm to 243.02 nm with a step size of 2.56×10^{-4} nm (this is the minimum step size possible, corresponding to a frequency step size of 1.32 GHz). For each laser pulse the ion and photon temporal signals were captured by the digital oscilloscope and transferred to a PC. The PC accumulated the signals for 50 laser shots at each wavelength and computed the average signals. Simultaneously the laser energy was recorded and the average intensity of the 50 laser pulses was determined. The wavelength scans have been measured for ten different laser intensities ranging from 1 to 340 MW/cm^2 and for both advanced and delayed extraction fields. Numerical data analysis was employed to integrate the ion and photon yields over time to obtain the total average ion and photon yield per laser pulse as a function of laser detuning. Because the temporal profiles are recorded as voltages by the oscilloscope, the unit for the vertical scale in the time-of-flight spectra is volt, and the total yields are in volt$\times$second.

Intensity scans were obtained by setting the laser to a fixed wavelength in the vicinity of the $1S_{1/2}$-$2S_{1/2}$ resonance and recording the ion and photon temporal signals as a function of laser intensity. Again the average signals for 50 laser pulses were calculated, and numerical data analysis was employed to integrate the ion and photon yields over time to obtain the total average ion and photon yields per laser pulse.

The alignment of the laser beam through the interaction region must be done with care to minimize the scattering of laser light in the vacuum chamber. A small fraction of 243 nm laser photons was observed by the Lyman-α photon detector. This scattered laser light is taken into account when calculating the Lyman-α temporal profiles in the wavelength scans.

The wavelength reproducibility of the laser is important for a meaningful comparison between wavelength scans at different laser intensities. The reproducibility was examined by conducting consecutive wavelength scans through the resonance at a fixed value of laser intensity. It was found that small drifts of a few minimum wavelength steps occurred between some consecutive scans when the measurements were taken. For this reason the position of zero detuning (0 GHz) for each scan is chosen to correspond with the maximum total ion yield at lower laser intensities and with the maximum total photon yield at higher laser intensities.

Because the geometry of the transient plasma critically depends on the precise position of the laser beam in front of the exit of the discharge tube, the possibility of laser beam movement in the interaction region due to the movement of the nonlinear crystal was investigated. A UV-sensitized charge-coupled device (CCD) camera was positioned close to the interaction region. The laser beam position was monitored via the image produced by the camera, averaged over 50 laser shots. Images taken during a scan of the wavelength were carefully checked and it was determined that no detectable movement of the laser beam in the interaction region occurred.

III. RESULTS

A. Ion time-of-flight profiles

Figures 2 and 3 present ion time-of-flight spectra obtained from scans of the laser wavelength through the $1S_{1/2}$-$2S_{1/2}$ resonance. Wavelength scans have been performed for ten different laser intensities for both an advanced and a delayed extraction field. Figures 2 and 3 present spectra obtained at the highest laser intensities used: 340 MW/cm^2 for the advanced ion extraction field and 315 MW/cm^2 for the delayed extraction field. The laser detuning indicated in the figures is given in GHz and is the single photon detuning from the resonance. The zero position of the time scale is taken as the time at which the laser pulse finishes. Figures 2 and 3 show the various effects that occur as the laser is scanned through the $1S_{1/2}$-$2S_{1/2}$ resonance; to follow the scan one views the figures in the order 2(a)–2(f) and 3(a)–3(f).

The time-of-flight profiles in Fig. 2(a) display the differences associated with the two cases of ion extraction field timing relative to the laser pulse. At this detuning the profiles are not significantly affected by collective effects and the peaks occur at the same position as the benchmark times of 590 and 630 ns. These benchmark times are obtained from on-resonance measurements at very low laser intensities (<5 MW/cm^2) where collective effects are absent and only a single peak is observed in the ion time-of-flight spectra. The small difference in the time of flight for the two cases of

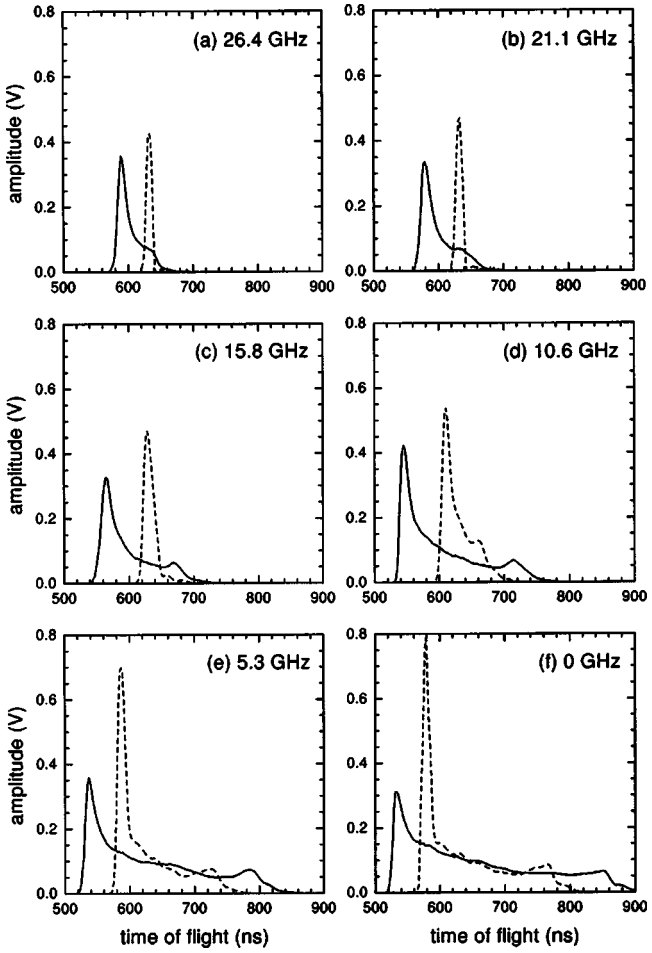

FIG. 2. Ion time-of-flight profiles at specific positive laser detunings: ——, profiles for an advanced extraction field at a laser intensity of 340 MW/cm^2; — — —, profiles for a delayed extraction field at a laser intensity of 315 MW/cm^2.

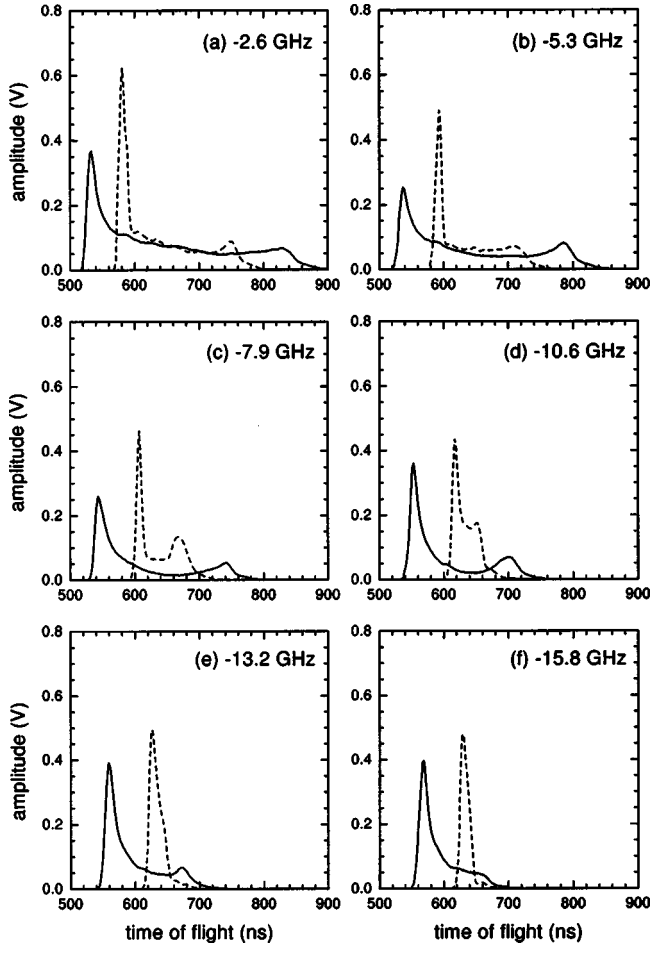

FIG. 3. Ion time-of-flight profiles at specific negative laser detunings: ——, profiles for an advanced extraction field at a laser intensity of 340 MW/cm^2; — — —, profiles for a delayed extraction field at a laser intensity of 315 MW/cm^2.

advanced and delayed ion extraction field is easily understood. When the extraction field is switched on before the laser pulse, the ions will move towards the detector as soon as they are created, thus arriving earlier than they would if the extraction field were applied immediately after the end of the laser pulse. This effect also explains the greater temporal width of the advanced field time-of-flight shape. In the case of the delayed field the ions are created and then accelerated as a bunch, thus leading to the observed narrower peak.

As the laser is tuned closer towards the $1S_{1/2}$-$2S_{1/2}$ resonance the shape of the time-of-flight profiles increase in total yield (the area under the time-of-flight profile) and in temporal width. The first ions arrive at the detector sooner as the laser is tuned closer to the resonance. On resonance at 0 GHz, see Fig. 2(f), the maximum amplitude and width occur and the first ions arrive 50 ns earlier in both the advanced and delayed extraction field cases. In the advanced extraction field case the temporal width of the ion time-of-flight profile is 360 ns, i.e., about six times the temporal width of the profile at the starting position of the scan. In the case of the delayed extraction field the ion profile expands up to 15 times its size at the starting position.

These features are characteristic of collective interactions in the transient plasma. An increase in temporal width and the early arrival of the first ions have been observed by Bowe *et al.* [3] in ion time-of-flight spectra recorded at zero detuning as a function of laser intensity. The measurements in Figs. 2 and 3 show similar behavior when the laser intensity is kept constant and the laser detuning is decreased towards the $1S_{1/2}$-$2S_{1/2}$ resonance.

As the laser passes through the resonance, the amplitude and width of the profiles at negative detunings decrease in a manner, which is different from the behavior noted on the positive detuning side. Comparison of Figs. 2(d) and 3(d) shows that significantly fewer ions reach the detector on the negative detuning side. This difference in the shapes of the ion time-of-flight profile leads to a strongly asymmetric wavelength profile, see Sec. III B. The time-of-flight profiles in this region will be examined in detail in Sec. III C.

B. Total ion and photon yields as a function of laser detuning

Figures 4, 5, and 6 present the total ion and photon yields obtained from scans of the laser wavelength through the $1S_{1/2}$-$2S_{1/2}$ resonance in atomic deuterium. As described in

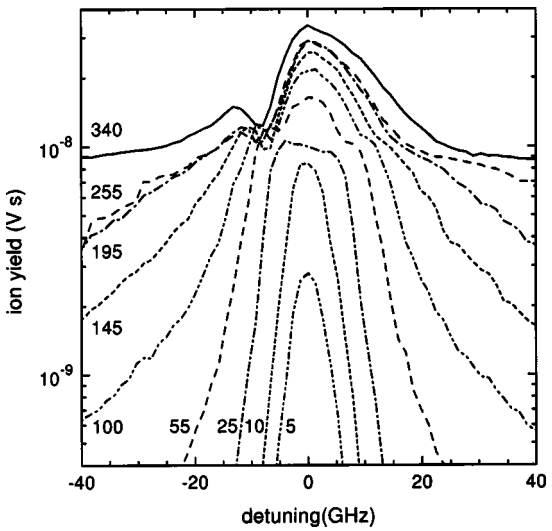

FIG. 4. Total ion yield versus laser detuning at various laser intensities. The ion extraction field is turned on before the laser pulse (advanced extraction field).

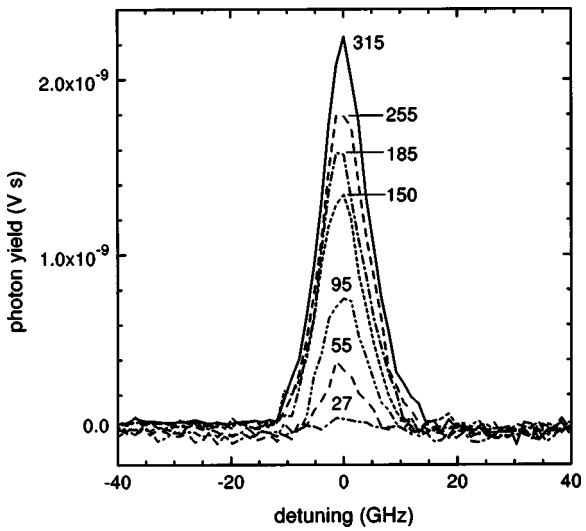

FIG. 6. Total photon yield versus laser detuning at various laser intensities. The ion extraction field is turned on after the laser pulse (delayed extraction field).

Sec. II the total yields are obtained by integrating the ion time-of-flight profiles and the photon temporal profiles over time. For instance, the integrals over each of the 12 advanced profiles in Figs. 2 and 3 correspond to 12 of the data points on the top curve in Fig. 4. For the sake of clarity, the total yields as a function of laser detuning will be referred to as detuning profiles in this paper. Detuning profiles have been measured for ten different laser intensities for both an advanced and a delayed extraction field. The laser detuning is given in GHz and is the single photon detuning from the $1S_{1/2}$-$2S_{1/2}$ two-photon resonance. Figure 6 shows the total photon yield for the delayed extraction field; the profiles for the advanced field are very similar and are not shown here.

Figures 4 and 5 show that significant physical effects occur as the laser intensity is increased. The overall width of the detuning profiles increases due to power broadening, but the profiles deviate from a Lorentzian profile and develop a significant asymmetry. These effects are attributable to the increasing influence of the collective interactions in the laser plasma as the laser intensity and hence charge density is increased. We first focus on the ion detuning profiles for the advanced field case in Fig. 4.

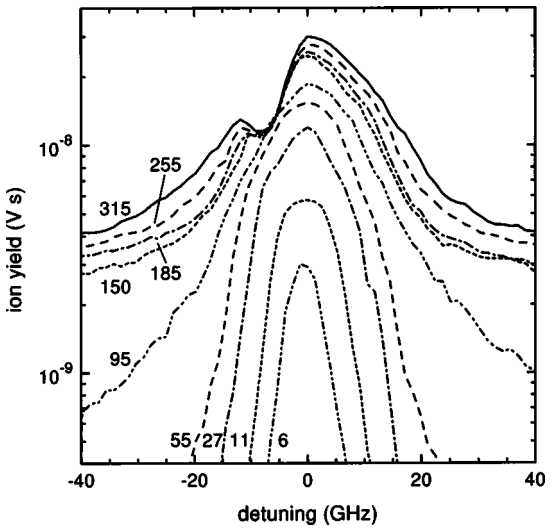

FIG. 5. Total ion yield versus laser detuning at various laser intensities. The ion extraction field is turned on after the laser pulse (delayed extraction field).

The detuning profiles at 1.3 MW/cm^2 (not shown in Fig. 4), at 5 MW/cm^2 and at 10 MW/cm^2 are symmetric around 0 GHz. At these laser intensities no broadening of the ion time-of-flight profiles was observed and no appreciable Lyman-α photon signal was detected. The results obtained at laser intensities of 10 MW/cm^2 and lower are representative of the interaction of a single atom with a perturbing light field, and collective effects are absent.

The detuning profiles at 25 MW/cm^2 and at 55 MW/cm^2 are more or less symmetric but show a profound deviation from a simple Lorenzian peak shape. For a small range of detunings (about ±5 GHz at 25 MW/cm^2 and ±8 GHz at 55 MW/cm^2) the time-of-flight profiles recorded at these intensities displayed an increase in temporal width due to collective effects. Over about the same range of detunings Lyman-α photon signals were detected. Once the yield of ions reaches the value of 1.0×10^{-8} V s, the ion detuning profiles show a significant change in shape. This critical level is observed in the flattened central peak of the detuning profile at 25 MW/cm^2, and in the shoulder in the right wing at 55 MW/cm^2. This level corresponds to a critical value of the charge density, above which the experimental results are modified by the collective interactions in the laser plasma.

At laser intensities of 100 MW/cm^2 and higher, the points where the ion yield reaches the critical value move further out into the wings of the ion detuning profiles to progressively larger detunings with increasing laser intensity. The ion detuning profiles develop significant asymmetry. Of particular interest is the dip, which develops on the left-hand side of the detuning profiles at -9 GHz. Figure 4 shows that

the dip occurs when the ion yield has reached the value of 1.0×10^{-8} V s. This clearly indicates that the asymmetry is linked with collective effects. This is also shown by the ion time-of-flight spectra, which show a significant broadening at those laser intensities and detunings where the total ion yield exceeds the critical value (discussed further in Sec. III C). At these laser intensities strong Lyman-α photon signals were detected, but notably there was no sign of any asymmetry in the photon detuning profiles recorded.

Similar features are observed in the ion detuning profiles in Fig. 5 for the delayed extraction field. The detuning profiles at 1.3 MW/cm^2 (not shown in Fig. 5) and at 6 MW/cm^2 are symmetric around 0 GHz and there are no collective effects. At 11 MW/cm^2 there are slight indications for the onset of collective effects. The detuning profile displays a slightly flattened shape around 0 GHz. The time-of-flight profiles measured at 0 GHz displayed a slight expansion in the temporal width of the profile, but no Lyman-α photon emission was observed above the background at this laser intensity.

The detuning profiles at 27 MW/cm^2, at 55 MW/cm^2, and at 95 MW/cm^2 are more or less symmetric around 0 GHz. For a small range of detunings (about ±5 GHz at 25 MW/cm^2, ±8 GHz at 55 MW/cm^2, and ±11 GHz at 95 MW/cm^2) the time-of-flight profiles display an increase in temporal width due to collective effects. Lyman-α photon signals are detected at 55 MW/cm^2 and at 95 MW/cm^2, see Fig. 6.

The critical level above which collective effects play a dominant role is less evident in the delayed detuning profiles than in the advanced detuning profiles. Examination of the ion time-of-flight spectra recorded at laser intensities and detunings for which the total ion yield is in the range 5×10^{-9} to 10^{-8} V s shows that there is a slight increase of the width of the profiles. This suggests that there is a more gradual transition into the regime of collective effects in the case of the delayed extraction field. When the total ion yield is above 10^{-8} V s, the widths of the ion time-of-flight profiles increase significantly.

At laser intensities of 150 MW/cm^2 and higher, the ion detuning profiles show a significant asymmetry. Again a dip develops on the left-hand side of the detuning profiles near -9 GHz, when the ion yield has reached the value of about 1.0×10^{-8} V s. In the advanced detuning profiles the dip shifts slightly further from the maximum of the ion yield as the laser intensity is increased, whereas in the delayed detuning profiles the dip stays at the same position.

The relationship between the density of ions n in the interaction region and the total charge Q measured by the detector is given by $n=Q/(e\eta GV)$, where e is the elementary charge, $\eta\approx0.3$ is the efficiency of the detector for detecting an ion, $G\approx4.5\times10^5$ is the gain of the detector, and $V\approx3\times10^{-5}$ cm^3 is the interaction volume in which the charges are produced. The total charge Q is obtained by integrating the ion time-of-flight profile recorded by the oscilloscope and dividing by the input impedance of the oscilloscope. Using these values, we obtain a critical charge density $n\approx3.0\times10^8$ cm^{-3} for the delayed field case. This value compares well with the critical charge density reported for sodium MPI transient plasmas [6]. It is less reliable to make a similar estimate for the advanced field case, because it is difficult to estimate the volume of the transient plasma at the end of the laser pulse in the case of an advanced extraction field. However, the fact that the critical ion yields in Figs. 4 and 5 are the same suggests that the critical charge density must be of the same order of magnitude in the advanced extraction field case.

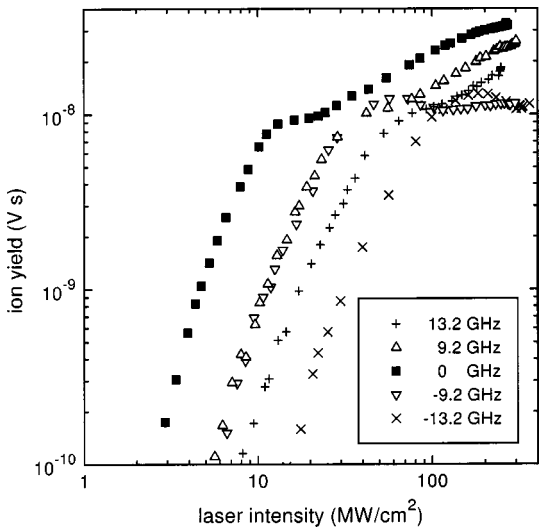

FIG. 7. Total ion yield versus laser intensity at specific laser detunings for an advanced extraction field.

The Lyman-α emissions in Fig. 6 are an indicator of the presence of large electric fields in the interaction region, which in the delayed field case cannot be due to the extraction field. There is no indication of any asymmetry in the detuning profiles. As the laser is tuned towards the resonance the Lyman-α temporal signal (and therefore the total yield of Lyman-α photons) increases dramatically. The emission coincides with the region where the ion time-of-flight profiles display maximum expansion. This is definitive evidence that large collective fields are generated in the laser plasma. It demonstrates the effectiveness of the collective field in Stark mixing the $2S_{1/2}$ level with the $2P_{1/2}$ and $2P_{3/2}$ levels.

C. Total ion and photon yields as a function of laser intensity

In order to elucidate the origin of the structure observed on the left-hand side of the detuning profiles displayed in Figs. 4 and 5, the ion yield as a function of laser intensity was determined at various detunings from the maximum of the $1S_{1/2}$-$2S_{1/2}$ resonance. These measurements recorded the ion time-of-flight profile as a function of laser intensity for fixed values of the laser detuning. From these measurements, total yields were obtained by integrating over the temporal profiles. The total ion yields are shown in Fig. 7 for the advanced extraction field and in Fig. 8 for the delayed extraction field.

The plots for the advanced extraction field in Fig. 7 reveal some interesting features. The same general behavior is evident in all five plots. At lower laser intensities the ion yields increase to the third power of the laser intensity. When the ion yield reaches the critical value of 1.0×10^{-8} V s the be-

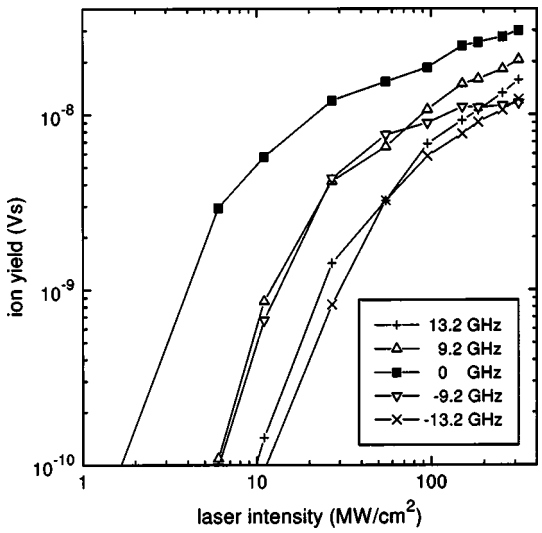

FIG. 8. Total ion yield versus laser intensity at specific laser detunings for a delayed extraction field.

havior changes dramatically in all five cases. Thus the importance of the critical charge density is once again emphasized. The detunings of $+9.2$ GHz and -9.2 GHz are of particular interest. As can be seen from Fig. 4, the position at -9.2 GHz corresponds to the point where the total ion yield drops to a local minimum. The position $+9.2$ GHz is simply chosen because it is the same detuning on the opposite side of the resonance. It can be seen in Fig. 7 that the ion yield for both detunings increases at an identical rate up to the critical value. Above this value the two curves diverge appreciably. The $+9.2$ GHz curve continues to rise, albeit at a reduced rate. The -9.2 GHz curve, however, turns over completely and the ion yield actually drops before making a slight recovery towards nearly complete saturation. Similar behavior is noted in the $+13.2$ and -13.2 GHz curves. These curves again highlight the asymmetry observed in the detuning profiles in Figs. 4 and 5.

The plots for the delayed extraction field in Fig. 8 show similar features as the plots for the advanced extraction field. At lower laser intensities the ion yields increase to the third power of the laser intensity, and above the critical value of 1.0×10^{-8} V s the ion yields begin to saturate. As already noted in Sec. III B the critical yield is less well defined in the delayed field case. The development of the asymmetry at high laser intensities is again observed: above 100 MW/cm^2 the $+9.2$ GHz curve continues to rise at a reduced rate, whereas the -9.2 GHz curve shows nearly complete saturation.

A set of ion time-of-flight profiles for increasing laser intensities is shown in Fig. 9. The measurements are recorded using an advanced extraction field at detunings of -9.2 and $+9.2$ GHz. At the lowest intensity (21 MW/cm^2) the time-of-flight profiles are very alike. However, as the intensity is increased, the time-of-flight profiles at negative detunings show both quantitative and qualitative differences. In particular the second peak becomes larger and the temporal width becomes less than the profiles of equivalent intensity on the positive detuning side. At -9.2 GHz detuning far

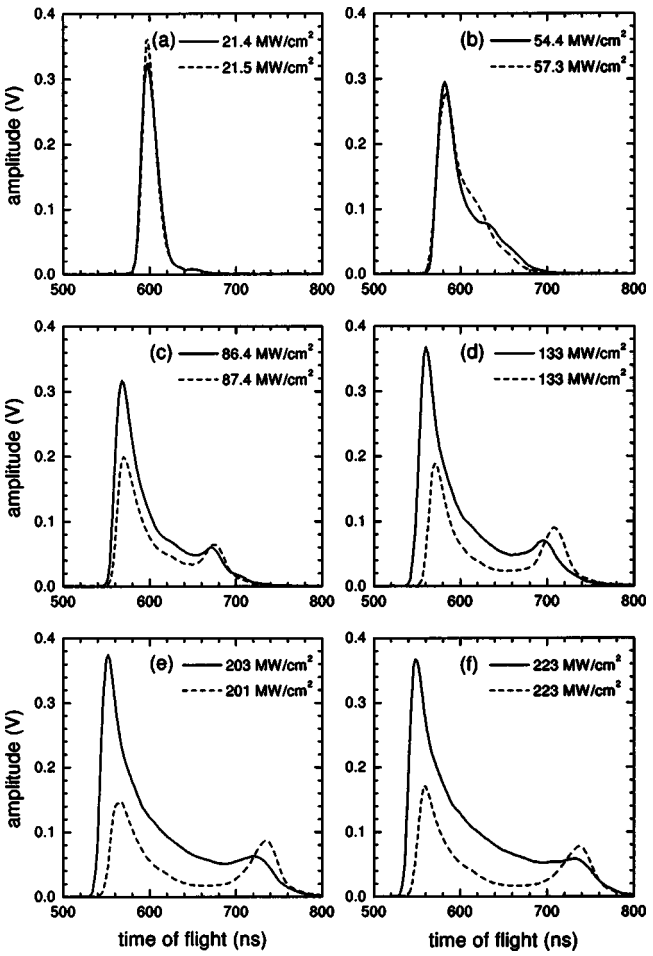

FIG. 9. Ion time-of-flight profiles for an advanced extraction field recorded for several different laser intensities: ——, profiles measured at a detuning of $+9.2$ GHz; $-\ -\ -$, profiles measured at a detuning of -9.2 GHz.

fewer ions reach the detector: the second peak contains more ions, but fewer ions are found in the central region and in the first peak. At 223 MW/cm^2 in Fig. 9(f) the total ion yield integrated over time at -9.2 GHz is 50% less than at $+9.2$ GHz. This reduction of the total ion yield at -9.2 GHz also manifests itself in the dip in the detuning profiles of Fig. 4.

IV. DISCUSSION

By examination of the experimental data it has been possible to identify the onset of collective effects. The magnitude of the collective effects is directly related to the ion and electron charge densities. The ion time-of-flight profiles and the Lyman-α photon temporal profiles provide direct evidence of the presence of collective interactions. In particular the growth in the temporal width of the ion time-of-flight profiles as a function of laser intensity and detuning illustrate the collective interactions. By controlling the experimental parameters (laser intensity and detuning) it is possible to control the magnitude of the collective electric field in the interaction region and its effectiveness in Stark mixing the $2S_{1/2}$ level with the $2P_{1/2}$ and $2P_{3/2}$ levels.

Of particular interest is the peak-dip structure which de-

velops on the left-hand side of the detuning profiles for both cases of the ion extraction field (Figs. 4 and 5). The secondary peak cannot simply be attributed to the $2P_{1/2}$ state. This state has lower energy than the $2S_{1/2}$ state and hence would be found to the left of the zero of the detuning scale. However, the energy separation of these states is 1.0 GHz in an electric field free environment and about 6 GHz for an electric field strength of 2000 V/cm. Considering the laser bandwidth of 10 GHz at 243 nm and the step size of 1.32 GHz, it is unlikely that the laser could resolve the $1S_{1/2}$-$2S_{1/2}$ structure. There is no sign of this structure in the Lyman-α yields in Fig. 6. If the left-hand structure were an atomic feature due to the collective field enabling effective population of the $2P_{1/2}$ level then some sign of this could be expected in the Lyman-α signal. Thus it seems unlikely that the structure on the left-hand side is attributable to the $2P_{1/2}$ state.

Careful comparison of the shape of the ion time-of-flight profiles in Fig. 9 indicates that there are both qualitative and quantitative differences between the two sets of profiles. A large number of ions are missing from the first peak and central region of the time-of-flight profile in the vicinity of the dip. The measurements in Figs. 7 and 8 dramatically illustrate the difference in behavior between the total ion yield at detuning positions in the vicinity of the dip and positions of equal detuning on the opposite side of the resonance. In the dip the yield of ions saturates and even decrease as the laser intensity is increased.

There are two possible reasons for these ''missing'' ions. The first possibility is that the Coulomb expansion of the ion cloud and the associated loss of detected ions are somehow enhanced at detunings around -9 GHz. However, if this were true, then one would expect to see a greater temporal width for the ion time-of-flight profiles at negative detunings (Fig. 9), whereas the opposite is actually observed. Because the magnitude of the Coulomb expansion of the ion cloud is directly related to the charge density, one would also expect that collection losses would be greater at the resonance than in the wings of the detuning profile.

The second possibility is that rather than being lost the ions are not produced in the first place. The structure may be due to the collective field ''detuning'' the atoms from the laser. As the laser intensity and hence charge density increases, the collective field shifts the $2S_{1/2}$ level with respect to the fixed position of the laser frequency. The $2S_{1/2}$ level shifts towards higher energies as a function of electric field strength. Therefore, if the laser is tuned to a fixed position to the left of the zero position of the $1S_{1/2}$-$2S_{1/2}$ resonance, the shift associated with an increasing collective field could essentially ''detune'' the atom from the laser, thus leading to a decrease in the ion yield. On the opposite side of the resonance the collective field induced shift could enhance the ion yield by reducing the detuning between the $2S_{1/2}$ level and the laser.

The change in shape of the time-of-flight profiles at -9.2 GHz in Fig. 9 provides unambiguous evidence for the coupling of the atomic photoionization process to the formation and time-evolution of the transient plasma. If there were no such coupling and the transient plasma would primarily be determined by the total number of ions produced during the laser pulse, one would expect to be able to find a detuning elsewhere near the resonance where the number of ions generated would be equal, and where the time-of-flight profile would be identical in shape. No such detuning can be found. The asymmetry in the ion detuning profiles is definitely a plasma structure related to the Stark mixing of the $2S_{1/2}$, $2P_{1/2}$, and $2P_{3/2}$ levels. Due to the complicated convolution of atomic and plasma processes present, this asymmetry is difficult to understand in terms of a simple qualitative model.

In addition to Stark mixing, the collective field induces two effects that can seriously affect the evolution of charged yields, i.e., the Coulomb expansion and the electron trapping. In this section we outline the main features of these phenomena, and by using simple arguments we estimate the order of magnitude of the charge density at which a relevant departure from the behavior of uncoupled charges may occur. First, we analyze the expansion of a spherical and uniformly charged cloud of initial radius d. To account for the finite production time, especially in our case since ionization is induced by a 13 ns laser pulse, we assume a simple three-photon process, the rate of which is given by

$$\frac{dN_i}{dt} = \alpha I_L^3(t)(N_0 - N_i), \tag{1}$$

where N_0 is the gas density and α the probability of ionization. The laser intensity is given by $I_L(t) = I_0 g(t)$, where I_0 is the laser peak intensity and $g(t)$ is the temporal shape. Equation (1) can be integrated to give

$$N_i(t) = N_0\left(1 - \exp\left[-\alpha I_0^3 \int_0^t g^3(t)dt\right]\right). \tag{2}$$

The internal field, in spherical symmetry, of a uniformly charged cloud is

$$E_{\text{int}} = \frac{eN_i}{3\varepsilon_0} r,$$

where r is the distance from the center of the sphere. As a consequence, an ion placed on the surface of the sphere undergoes an acceleration given by

$$\frac{d^2r}{dt^2} = \frac{e^2 N_i}{3\varepsilon_0 M} r = \frac{1}{3}\omega_{pi}^2 r, \tag{3}$$

where $\omega_{pi}^2 = e^2 N_i / \varepsilon_0 M$ is the ion plasma frequency. The initial conditions are $r(0) = d$ and $dr/dt|_{t=0} = 0$.

Figure 10 shows an example of the influence of Coulomb expansion on the final charge density at the end of the laser pulse. We assume a gas density of 2×10^{12} atoms/cm^3, i.e., the maximum density encountered in our experiment. For convenience, the peak laser intensity is referred to the saturation intensity I_s, i.e., the intensity at which the argument of the exponential in Eq. (2) after integration over the laser time shape is equal to 1. This is high enough to achieve total ionization at the end of a laser pulse of 13 ns. Dashed and solid lines represent the charge density $N_i(t)$ solution of Eq. (1) for $I_0 = I_s$ and $I_0 = 10 I_s$, respectively. Dash-dot-dot and

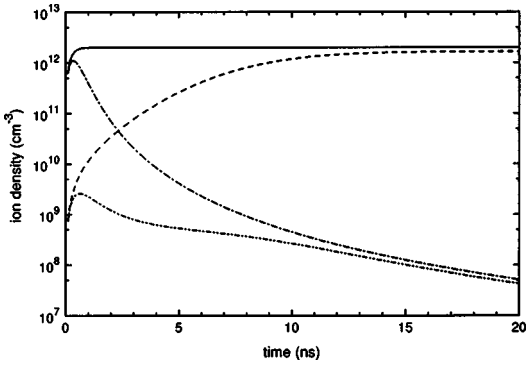

FIG. 10. The effect of Coulomb expansion on a spherical charge cloud of uniform charge density. Legend: — — —and ——, the charge density as a function of laser pulse duration in the absence of Coulomb expansion for $I_0=I_s$ and $I_0=10I_s$, respectively (see text); –··–·· and –·–·, the charge density in the presence of Coulomb expansion for $I_0=I_s$ and $I_0=10I_s$, respectively.

dash-dot lines correspond to the charge density in the presence of Coulomb expansion, i.e., $N_i(t)(d/r)^3$, for $I_0=I_s$ and $I_0=10I_s$, respectively.

The curves in Fig. 10 show that the effective density at the end of the laser pulse is several orders of magnitude less than the value due to the multiphoton process. In this example, the radius of the initial charged cloud increases by about a factor of 10. It explains the increasing widths of the recorded ion time-of-flight profiles as the laser intensity, i.e., the charge density, increases. The above simple model is useful to investigate some of the features of the phenomenon under study.

Equations (2) and (3) emphasize the nonlinear character of the plasma evolution. It is evident that the geometry of the charged cloud is relevant since it affects the intensity and shape of the collective field. Recall that Eq. (3) is valid only under the assumption of a spherical, uniformly charged cloud. In a cylindrical geometry, neglecting the axial contribution, the numerical factor 1/3 must be replaced by 1/2 and hence it leads to an enhancement of the spread. The geometry of our experiment is more complicated due to the presence of the extraction field. When the field is applied at the end of laser pulse, the source of ionization, i.e., the three-photon process, has a radial symmetry because of the laser spatial intensity distribution around the laser beam axis. When the extraction field is on during the laser pulse, it breaks the symmetry since it is directed perpendicularly to the laser beam axis. The behavior of measured quantities when the extraction field is applied before or after the laser pulse is rather similar apart from differences that can be ascribed to a different rate of ionization (at the same laser detuning). This leads one to infer that the break of symmetry has a weak effect on the charge propagation. This problem, however, can only be solved by a much more detailed and sophisticated numerical modeling.

An approximate criterion for the critical charge density, at which the ion expansion is dominated by the Coulomb expansion, can be carried out by comparing the time of Coulomb expansion, i.e., $1/\omega_{pi}$, with the time of thermal expansion $\tau_{thi}=d\sqrt{M/(2kT_i)}$, according to Ref. [1]. In practical units, it leads to $N_i \geqslant (1.5\times10^6)T_i(\mathrm{eV})/d^2$ ions/cm^3. In our experiment, ions at room temperature are produced in a spot of radius $d=100\ \mu$m, which leads to $N_i \geqslant 4\times10^8$ ions/cm^3, in excellent agreement with the experimentally measured critical density of 3×10^8 ions/cm^3 (Sec. III B).

Following this simple approach, we estimate the order of magnitude of the charge density threshold at which electron trapping starts to play a role. Consider first the case of a delayed extraction field where in principle one can suppose a more relevant role of this phenomenon. At the beginning of the laser pulse, electrons expand with the thermal velocity $v_e=\sqrt{2kT_e/m}$, where kT_e is given by the energy conservation in the three-photon process, i.e., $kT_e=1.7$ eV. Trapping would occur if the maximum value of the Debye length

$$\lambda_D=\left(\frac{\varepsilon_0 T_e}{e^2 N_i}\right)^{1/2}$$

calculated at the center of charge profile (assuming $n_e=N_i$), is less than the width of the interaction region. In our case, this leads to $N_i>10^{10}$ ions/cm^3. However, as demonstrated in Ref. [24], this parameter does not give a realistic picture of charged clouds produced by multiphoton ionization. In fact, in the presence of strong density gradients, as in our case where the laser beam waist has a spot radius of 100 μm, and a relatively long production time, i.e., on the nanosecond scale, the electrons rapidly leave the interaction region and hence their profile spreads out. For instance, an electron with an initial energy of 1.7 eV, as in our experiment, travels by about 1 cm during the laser pulse. In addition, when the charge density is high enough, electrons spread out because of the Coulomb repulsion whose time scale is now given by the electronic plasma frequency $\omega_{pe}=(M/m)^{1/2}\omega_{pi}$. Practically, it is equivalent to rescale the time scale of Fig. 10 by multiplying by $(m/M)^{1/2}\approx1.6\times10^{-2}$. As a consequence, the ion field is unscreened by the surrounding electrons, which are distributed over a very large area, and the ion Coulomb repulsion takes place unperturbed as described in the above model. When the extraction field is applied, the field generated by the ions would compete to prevent electrons from collection by the repeller (the metal plate surrounding the tip of the discharge source, see [3]). By using the definition of the ion field given above, one can find that this would occur for a density $N_i \geqslant 3\varepsilon_0 E_0/ed\approx10^{11}$ ions/cm^3. The data in Fig. 10 show that at the end of the laser pulse the ion density, although close to much higher values at the first instants of laser pulse, is strongly reduced by the unscreened ion inner repulsion to a value several orders of magnitude less. Hence the electrons are rapidly collected by the extraction field. One can see from Fig. 10 that in the case of an advanced extraction field, also for $10I_s$, the ion density drops below the trapping value of 10^{11} ions/cm^3 in a few nanoseconds. Therefore, one can assert that in our experimental conditions the electron trapping plays a negligible role, although it was observed by Giammanco [4] by using a weak extraction field (about 30 V/cm).

V. CONCLUSION

A systematic study of collective effects in the multiphoton ionization of atomic deuterium has been undertaken. This has been achieved by performing measurements of both the temporal profiles and total yields of the ions and photons emanating from the laser-produced transient plasma. The primary method of investigation has been the scanning of the laser wavelength through the $1S_{1/2}-2S_{1/2}$ resonance. The data acquisition system enabled simultaneous measurement of the ion and photon signals.

A critical charge density of 3×10^8 ions/cm^3 has been identified, above which the experimental results are dominated by collective interactions. This critical charge density is independent of the detuning of the laser, indicating that this density is independent of the multiphoton process generating the plasma. Evidence for collective effects have been observed in the anomalous saturation of the ion yields and the increase in temporal width of the ion time-of-flight profiles. The effectiveness of the collective field in Stark mixing the $2S_{1/2}$ level with the $2P_{1/2}$ and $2P_{3/2}$ levels has been demonstrated by the observed Lyman-α emissions.

Anomalous structure, in the form of a dip in the total ion yield as a function of laser detuning, has been observed on the negative detuning side of the resonance. The difference between the transient plasmas produced at ±9 GHz detunings is also observed in the ion time-of-flight profiles and in the saturation of the total ion yields at laser intensities above 100 MW/cm^2. These observations provide unambiguous evidence for the coupling between the atomic multiphoton ionization process and the formation and time evolution of the transient plasma.

ACKNOWLEDGMENTS

This work has been supported by the Scientific Research Program and the International Collaboration Program of Enterprise Ireland. The authors would like to acknowledge Professor R. W. McCullough for helpful discussions on this work and Mr. David Watson for expert technical support. One of the authors (B.J.S.) gratefully acknowledges receipt of support from the National University of Ireland, Maynooth.

[1] *Plasma Collective Effects in Atomic Physics*, edited by F. Giammanco and N. Spinelli (Edizioni ETS, Pisa, 1996).
[2] M. V. Ammosov, Laser Phys. **4**, 431 (1994).
[3] P. Bowe, F. Giammanco, R. W. O'Neill, P. J. M. van der Burgt, and J. A. Slevin, Phys. Rev. A **58**, 1389 (1998).
[4] F. Giammanco, Phys. Rev. A **40**, 5160 (1989).
[5] E. Arimondo, C. E. Burkhardt, F. Giammanco, L. J. Qin, and A. Vellante, Opt. Commun. **71**, 52 (1989).
[6] F. Giammanco and E. Arimondo, Eur. Phys. Lett. **11**, 31 (1990).
[7] F. Fabre, G. Petite, P. Agostini, and M. Clement, J. Phys. B **15**, 1353 (1982).
[8] L. A. Lompré, A. L'Huillier, G. Mainfray, and C. Manus C, J. Opt. Soc. Am. B **2**, 1906 (1985).
[9] L. A. Lompré, G. Mainfray, C. Manus, and J. Kupersztych, J. Phys. B **20**, 1009 (1987).
[10] T. J. McIlrath, P. H. Bucksbaum, R. R. Freeman, and M. Bashkansky, Phys. Rev. A **35**, 4611 (1987).
[11] X. Xing, D. Charalambidis, and C. Fotakis, Opt. Commun. **79**, 181 (1990).
[12] D. Charalambidis and X. Xing, J. Phys. B **24**, 127 (1991).
[13] M. V. Ammosov and A. A. Zhuk, Laser Phys. **2**, 928 (1992).
[14] F. Giammanco, G. Arena, R. Bruzzese, and N. Spinelli, Phys. Rev. A **41**, 2144 (1990).
[15] F. Giammanco, M. Armenante, V. Beradi, N. Spinelli, and R. Velotta, Phys. Rev. E **47**, 1960 (1993).
[16] R. Velotta, L. Avaldi, R. Camilloni, F. Giammanco, N. Spinelli, and G. Stefani, Phys. Rev. A **54**, 2482 (1996).
[17] M. V. Ammosov, J. Opt. Soc. Am. B **8**, 2260 (1991).
[18] T. Ditmire, Contemp. Phys. **38**, 315 (1997).
[19] F. Giammanco, Phys. Rev. A **43**, 6939 (1991).
[20] S. C. Miller and R. F. Haglund, *Laser Ablation* (Springer, Berlin, 1991).
[21] G. DelGobbo, F. Giammanco, F. Maccarrone, P. Marsili, and F. Strumia, Nuovo Cimento D **18**, 791 (1996).
[22] G. DelGobbo, F. Giammanco, F. Maccarrone, P. Marsili, and F. Strumia, Appl. Phys. B: Lasers Opt. **64**, 349 (1997).
[23] F. Giammanco, Phys. Rev. A **36**, 5658 (1987).
[24] F. Giammanco, Phys. Rev. A **40**, 5171 (1989).
[25] M. V. Ammosov, F. A. Ilkov, M. G. Malakhov, and Ch. K. Mukhtarov, J. Opt. Soc. Am. B **6**, 1961 (1989).
[26] *Low Temperature Plasma Physics*, edited by R. Hippler, S. Pfau, M. Schmidt, and K. H. Schoenbach (Wiley-VCH, Berlin, 2001).
[27] S. Trajmar and J. C. Nickel, Adv. At., Mol., Opt. Phys. **30**, 45 (1993).